

## Active Control of Large-Scales in a High-Reynolds-Number Turbulent Boundary Layer

Z. Ruan, W. J. Baars, M. R. Abbassi, N. Hutchins and I. Marusic

Department of Mechanical Engineering  
University of Melbourne, Victoria 3010, Australia

### Abstract

The relationship between large-scale structures and near-wall turbulence in both canonical and perturbed high Reynolds number turbulent boundary layers ( $Re_\tau = 14400$ ,  $U_\infty = 20$  m/s) is investigated experimentally. A spanwise array of hot-film probes and wall-normal jets are placed  $1.7\delta$  apart in the streamwise direction to observe, and selectively perturb, large-scale events in the logarithmic region with the implementation of different control strategies. Using a further spanwise array of hot-films and a traversing hot-wire probe downstream of the actuators, we evaluate the influence of the modified large-scale structures on the wall-shear stress fluctuations. In terms of flow control, it is anticipated that the maximum skin-friction reduction with the current control infrastructure is bounded at 4.5%. Owing to the imperfection of the actuation process, this value fails to match the potential 8% mean-wall-shear-stress contributed by the large-scale motions and very large-scale motions with streamwise wavelength greater than  $1.5\delta$  in the turbulent boundary layer at  $Re_\tau = 14400$ , which is extrapolated based on the relationship between the large-scale turbulence energy variation for each perturbed boundary layer and their corresponding skin-friction drag change.

### Introduction

A turbulent boundary layer (TBL), occurring when fluid flows over a solid surface, is the thin region immediately adjacent to wall, which accounts for a significant portion of drag in a vast number of engineering applications. Leschziner *et al.* [10] estimate that one percent frictional drag reduction is equivalent to a million tonnes of fuel consumption and five million tonnes of greenhouse gas emission annually in the global aviation industry. These huge economic and environmental benefits have prompted research into many innovative turbulent control techniques, which have successfully reduced the turbulence skin-friction drag in low Reynolds number TBLs [4]. These turbulent control strategies mainly exploit the near-wall coherent structures, responsible for a majority of the turbulence energy production and consequently, the skin-friction in low Reynolds number TBLs [4]. However, most of these techniques suffer performance deterioration as the Reynolds number increases to the practical engineering regime ( $Re_\tau \approx O[10^5]$ ) [6].

In recent decades, studies have revealed the existence of large-scale motions (LSMs) and very superstructures/large-scale motions (VLSMs) within the logarithmic and outer region of high Reynolds number TBLs with  $Re_\tau$  greater than 1700 [8]. In practical engineering TBLs at high Re numbers, LSMs and VLSMs play important roles in the generation of large-scale turbulence energy, which can be reflected as the outer peak in the energy spectrogram [8]. More importantly, these large structures interact with the near wall turbulence via both superimposing upon their signature and modulating the small-scale near-wall turbulence. [8, 11]. Hutchins *et al.* [9] also reported the correlation between the large-scale streamwise velocity fluctuations and their footprints on the wall, such that low-velocity large-scale events are strongly associated with low-shear-stress at the wall.

Quantifying the influence of LSMs and VLSMs on skin-friction generation remains a challenge. Recently, a novel experiment conducted by Abbassi *et al.* [1] achieved a maximum local skin-friction drag reduction up to 3.2% via weakening the high-velocity large-scale structures using a spanwise array of wall normal jets. Giovanetti *et al.* [7] reported that LSMs and VLSMs are responsible for a 5–8% total skin-friction reduction in a LES channel flow at  $Re_\tau \approx 4000$ . In contrast, Deck [5] revisited the FIK identity and argued that the structures with a streamwise wavelength  $\lambda_x > \delta$  contribute to more than 48% of the mean skin-friction coefficient  $C_f$  at  $3060 < Re_\theta < 13650$ . A series of experiments are carried out in the current study to perturb the large-scale structures in different manners. By establishing the relationship between the large-scale energy and skin-friction variations, this paper investigates the potential of attaining drag reduction in high Reynolds number TBL via control of the large-scale streamwise velocity fluctuations. At the same time, the relationship between reduction of large-scale energy and the amplitude of the small scale fluctuations near the wall is also explored.

### Experiment Set-up

Experiments are conducted in the High Reynolds Number Boundary Layer Wind Tunnel (HRNBLWT) at the University of Melbourne. The measurements are performed at a nominal Reynolds number  $Re_\tau = 14400$  ( $U_\infty = 20$  m/s), with the boundary layer thickness  $\delta = 0.365$  m. Figure 1 provides a schematic of the experimental set-up. The boundary layer is tripped by a strip of P40 grit sand paper immediately after a 6.2 : 1 contraction section. The control infrastructure, with the same configuration as Abbassi *et al.* [1], employs two spanwise arrays of nine Dantec 55R47 glue-on-type hot-film sensors and nine wall normal jets with 2 mm  $\times$  50 mm rectangular slits. The upstream hot-films (the detection array) are positioned 19.8 m downstream of the tripped inlet to the working section, and there is a streamwise separation of  $\Delta x/\delta = 1.7$  between the wall normal jets (actuation array) and the detection array to accommodate the latency in real-time control.

Real-time low-pass filters with cut-off wavelength of  $\lambda_c = 1.5\delta$  convolute the upstream friction velocity fluctuation measured by the detection array to estimate the large-scale motions for actuation. Three different filters are investigated, including (i). a **Gaussian filter** with the standard deviation equivalent to one sixth of the  $1.5\delta$  filter length; (ii). a linear stochastic estimated filter (**LSE Filter**) designed based on the linear transfer function between the  $U_\tau$  signal from the detection array and the velocity fluctuations measured in the logarithmic region above the jets; (iii). a **2-D filter** which extracts only the two dominant spanwise Fourier modes based on the streamwise LSE filter. Furthermore, three different control algorithms are implemented, referred to as **reinforcing**, **desynchronizing** and **opposing** control, which interpret the estimate signal and employ the jets to target low-speed, random and high-speed large-scale structures, respectively. A clip of the control signals obtained in real-time measurement is provided in figure 1(c) showing the raw, filtered and actuation binary signals for the opposing scheme.

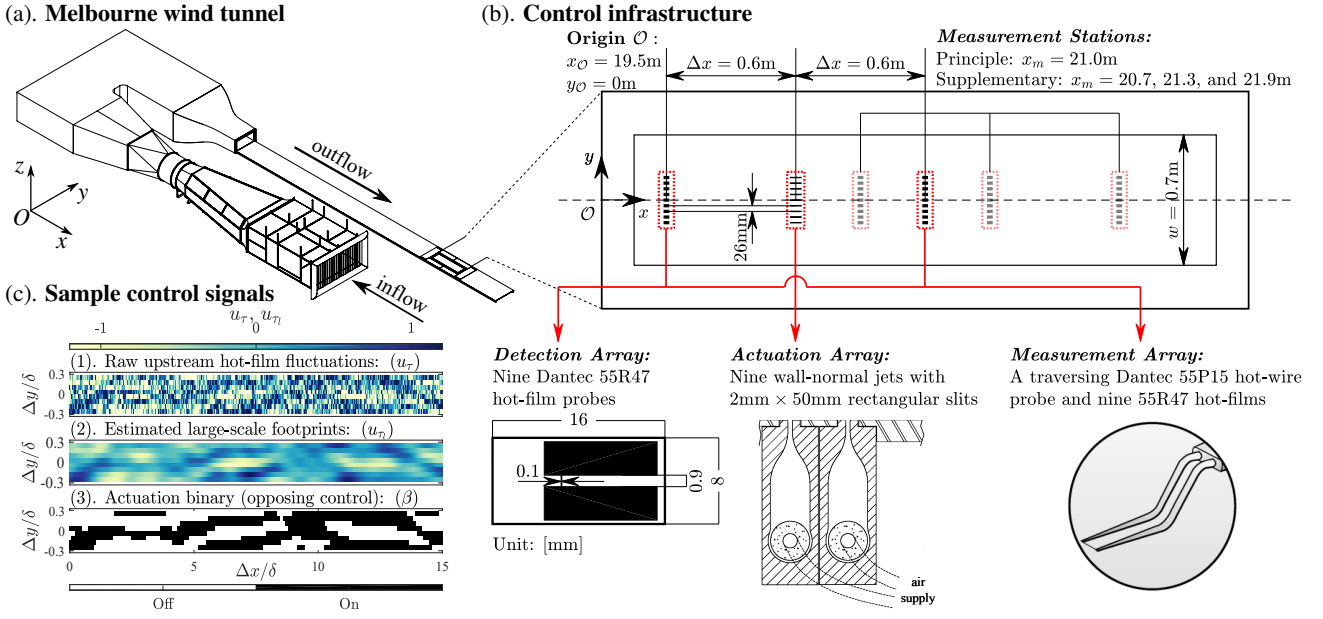


Figure 1: (a) Schematic of the HRNBLWT at the University of Melbourne (adapted from Baars et. al [2]); (b) Layout of the control infrastructure for the large-scale control experiments, starting at  $x_O = 19.5\text{m}$ , with the specification of all elements in detection, actuation and measurement arrays highlighted; (c) A clip of the real time control signals, including **1.** detected upstream skin-friction velocity field, **2.** estimated large-scale fluctuation field, and **3.** actuation binary signal for wall-normal jets.

The five control strategies investigated are summarized in table 1. The four measurement stations downstream of the actuators at  $\Delta x/\delta = 0.85, 1.7, 2.5$  and  $4.2$  as shown in figure 1(b), provide the ability to monitor the modified skin friction velocity fluctuations (and mean) downstream of the actuation. This is supplemented by an automated traversing Dantec 55P15 boundary-layer hot-wire probe, which measures the streamwise velocity fluctuation at 40 logarithmically spacing points covering a range  $8 < z^+ < 1.5\delta^+$  above the central sensor in the spanwise array. The coordinate system adopted in this paper is illustrated in figure 1(a), with  $x, y$  and  $z$  denoting the streamwise, spanwise and wall-normal directions respectively. Total streamwise velocity and its mean value are indicated by  $U$  and  $\bar{U}$ , respectively. The fluctuating part of the streamwise velocity is  $u$ , with the large- and small-scale components, as determined from a cut-off filter at  $1.5\delta$ , denoted by  $u_l$  and  $u_s$ , respectively. Subscripts “un” and “co” represent the quantities in uncontrolled and controlled boundary layers. The nominal friction velocity is  $U_\tau = \sqrt{\tau_w/\rho} = 0.64\text{m/s}$  and the superscript “+” denotes inner-scale normalized parameters (i.e.  $u^+ = u/U_\tau$  and  $z^+ = zU_\tau/\nu$ ).

No.	Real-time filter	Control algorithm
1	Gaussian Filter	Reinforcing Control
2	Gaussian Filter	Desynchronizing Control
3	Gaussian Filter	Opposing Control
4	LSE Filter	Opposing Control
5	2-D Filter	Opposing Control

Table 1: A summary of implemented control schemes.

## Results and Discussions

Figure 2(a) demonstrates the local skin-friction drag reduction, defined as  $DR(\%) = -(\tau_{wco} - \tau_{wun})/\tau_{wun} \times 100$ , along the span,  $-0.3 < \Delta y/\delta < 0.3$ , of the entire control plane. The curves demonstrate the average  $DR(\%)$  from 16 independent 3-minute-realizations measured at the principal measurement array, where the maximum local skin-friction drag reduction is detected. All control strategies yield the highest  $DR(\%)$  at  $|\Delta y/\delta| = 0.21$ , which could be attributed to the edge effects of

the spanwise array. Figure 2(b) only considers the drag reduction percentage at the mid-point of the control plane ( $\Delta y/\delta = 0$ ). Since the total actuation input is held constant (jets are on for half of the time), the difference in  $DR(\%)$  is purely ascribed to the control accuracy, which Baars et al. [2] defined as the degree of true high-velocity structures at the actuation array successfully estimated by their low-pass filtered upstream footprints. By measuring the streamwise velocity fluctuations via

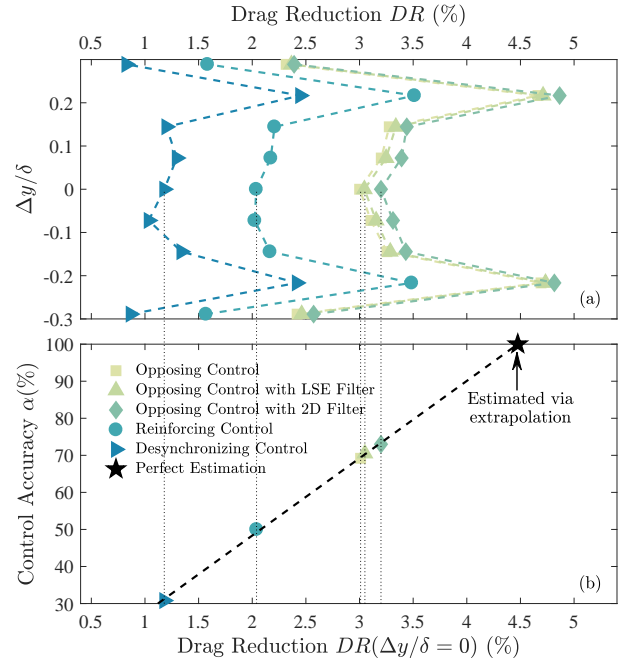


Figure 2: (a) The drag-reduction percentage measured by the hot-film array positioned at  $1.7\delta$  downstream of the actuation array for all control strategies performed in table 1; (b) The skin-friction drag reduction measured at the centerline of the control plane at  $1.7\delta$  downstream of the actuators with respect to the percentage of high-speed events manipulated.

a hot-wire positioned in the log-region above the actuation array simultaneously with the upstream hot-film array, the control accuracy  $\alpha$  for the opposing control with Gaussian filter is determined as 69.2%. The detection accuracy is improved by  $\sim 1\%$  when shaping the streamwise LSE filter based on the coherence spectrum between the skin-friction and streamwise velocity fluctuations at both sensor and actuation arrays [3]. Discarding the structures with a spanwise wavelength less than  $0.25\delta$ , because these are uncorrelated between the detection and actuation locations, results in a further increase of  $\alpha$  by 3%. It is worth noting that, by randomly engaging the jets, the desynchronizing control has a nominal  $\alpha = 50\%$  and, as the counterpart of the opposing control,  $\alpha$  of the reinforcing control is 30.8%. As figure 2(b) illustrated,  $DR(\%)$  at the centreline of the control plane is positively correlated with the control accuracy  $\alpha$ . By fitting the points with a linear curve (black dashed line) and extrapolating the line to  $\alpha = 100\%$ , it is hypothesized that the performance of large-scale control with a cut-off wavelength  $\lambda_c^+ = 20000$  via the current actuation process is bounded by 4.5%. This drag reduction compromises two major components.

The jet flow with upwards momentum, working as a “virtual wall”, prevents the down-wash motions of high-velocity large-scale structures from generating a local high shear-stress footprint on the wall. Hence, when a higher degree of high-speed large-scale motions is actuated on, the performance of the large-scale control will be enhanced. In addition to directly eliminating the high skin-friction footprints, another mechanism is related to the attenuated turbulent large-scale energy in the log-region due to the low-momentum jet flow. To further investigate such an effect, a spectral cut-off filter with a cut-off wavelength  $\lambda_c = 1.5\delta$  is applied to separate the streamwise velocity

$u$  into large- and small-scale fluctuations ( $u_l$  and  $u_s$ ). Figure 3(a) demonstrates the percentage change of the large-scale variance between the canonical and controlled boundary layers  $1.7\delta$  downstream of the actuation array. Percentage change is defined as  $\Delta u_l^2(\%) = (u_{lco}^2 - u_{lun}^2) / u_{lun}^2 \times 100$ , and is negative when the large-scale energy is reduced. In the viscous region ( $z^+ < 30$ ), the three opposing control strategies all achieve approximately 15% large-scale energy attenuation, with the 2-D filter performing better than the others. A limited energy increase appears in this region for the desynchronizing control, and the large-scale turbulence intensity has been increased by 15% for the reinforcing control where the negative fluctuations are strengthened. Such a phenomenon is more obvious in the logarithmic region,  $110 < z^+ < 2000$ , where the majority of large-scale energy resides. It is clear that the jet modification seems to penetrate to higher wall-normal locations ( $z^+ \approx 1500$ ) for the reinforcing control than for the opposing ( $z^+ \approx 800$ ). This is expected since the jets are predominantly firing into large-scale up-wash regions for the opposing case. Eventually, the curves for the different control scenarios collapse above the penetration height,  $z_p^+ = 3000$ . In contrast, using the same definition, the small-scale energy variation,  $\Delta u_s^2$ , show negligible variation between control strategies in figure 3(b). A mild 2%-5% small-scale energy reduction is obtained in the near-wall region ( $z^+ < 100$ ), whereas a dramatic energy increase occurs at the logarithmic region, which could be ascribed to the development of shear layers between the TBL and the jet in cross-flow.

From the trend observed in figure 3(a), figure 4(a) attempts to explore the relation between the mean drag reduction and the change in the intensity of the large-scale streamwise velocity fluctuations. Here we produce a scatter plot of the large-scale energy attenuation for each control strategy against corresponding mean skin-friction reduction, and we show this for all wall normal locations in the range  $5 < z^+ < 2000$  with the color-map indicating the  $z$  position. In general, the data for all control strategies plotted in this manner lies perfectly in the bounded grey band. The slope of the band implies that, as large-scale energy is increasingly attenuated, there is an increasing reduction in wall shear stress, although with an approximate limit suggest at 7.5% drag reduction for 100% attenuation of large-scale energy. It is noted that 2.1% drag reduction is achieved via the desynchronizing control strategy with little or no large-scale energy attenuation. This is due to the trivial injection of low momentum jet flows into the boundary layer in the desynchronized case. Hence, we might hypothesize that the effect on skin friction drag purely due to a 100% reduction in large scale turbulent energy, is a 5.4% reduction. In 4(a), we highlight the markers at  $z^+ = 15$  and 480 as pink and red, respectively, demonstrating that the large-scale energy attenuation at a specific wall-normal position is also linear related to the drag reduction. However, within the viscous region, the slope appears to be steeper. If we extrapolate this curve to 100% reduction, it would infer that larger drag reductions may be possible by more effectively controlling the large-scale fluctuations in the viscous region. Based on the slope of these two guidelines, a more conservative hypothesis would surmise that the turbulence energy with  $\lambda_x > 1.5\delta$  contributes approximately 4–8% of the mean skin-friction drag. Such a range meets the argument of Giovanetti *et al.* [7], who claimed a 5–8% frictional drag reduction when removing the LSMs and VLSMs through an artificial narrowing of the numerical domain.

We postulate that the observed correlation between the large-scale energy variation and the skin-friction drag reduction is related by the large-scale amplitude modulation and superposition effect of the large-scale energy onto the near-wall region

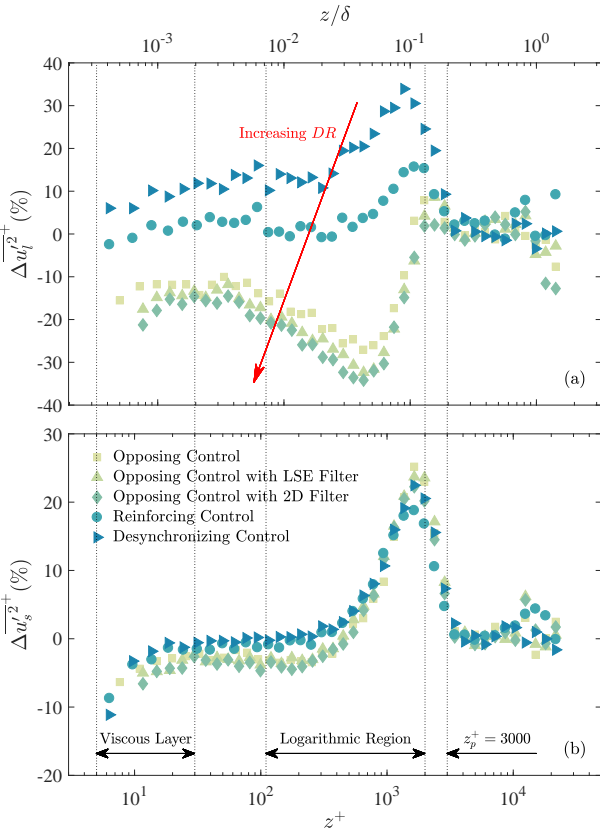


Figure 3: (a, b) The percentage variation of the large-scale and the small scale energy as a function of  $z^+$  for the perturbed boundary layers controlled via all strategies listed in table 1 at  $1.7\delta$  downstream of the actuation array.

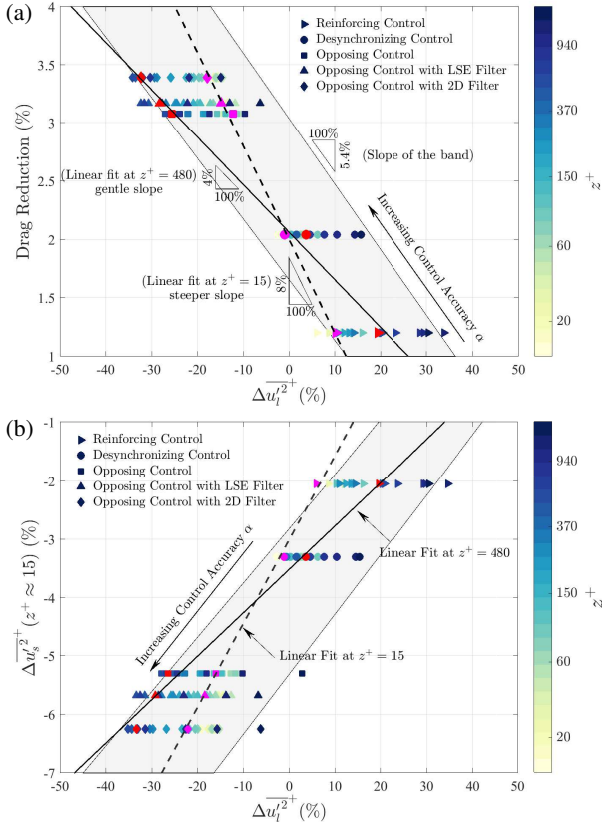


Figure 4: (a) Large-scale energy attenuation and drag reduction percentage for each control strategy with the color of the scatters indicating their  $z$  positions. The sloped band (the boundary layer) and the guidelines fitting the highlighted markers at  $z^+ = 15$  and 480 showing the influence of large-scales with  $\lambda_x > 1.5\delta$  on the skin-friction drag reduction; (b) The influence of the large-scale variance on the small-scale fluctuations based on the perturbed boundary layers controlled by different strategies in the same manner as (a).

[8, 11]. In figure 4(b), the effect of amplitude modulation is examined via investigating the variance of small-scale fluctuations in the viscous shear layer ( $10 < z^+ < 50$ ) and the large-scale energy attenuation at all  $z^+$  and for all control strategies in figure 4(a). The dashed and solid black lines demonstrate the relation between the change of small scale turbulence intensity and the change in large scale energy at the inner-peak ( $z^+ = 15$ ) and log region ( $z^+ = 480$ ), respectively. The steeper slope indicates the small-scale motions are rather more sensitive to the large-scale motions near the wall than the outer region. This follows the curve of the amplitude modulation coefficient, mentioned by Baars *et al.* [3], between the large-scale fluctuation and the small-scale envelope at different wall-normal positions.

## Conclusion

Experiments to actively control the large-scale structures in high Reynolds number TBLs were performed using a spanwise array of wall-normal jets. Oncoming large-scale structures are observed from their skin-friction velocity footprints extracted from a spanwise array of hot-film sensors via three different real-time low-pass filters. The observed LSMs and VLSMs with  $\lambda_x$  greater than  $1.5\delta$  are selectively perturbed and modified. It is observed that the variation of the fluctuating energy of the large-scale structures in a high Reynolds number TBL is linearly proportional to the percentage reduction of the skin-friction drag. Based on such a relationship, it is estimated that the removal of

LSMs and VLSMs with  $\lambda_x$  greater than  $1.5\delta$  could contribute up to 8% of the mean wall-shear-stress. However, since the current control strategy which manipulates only the high-velocity large-scale structures, is incapable of eradicating all large-scale turbulence energy, the maximum DR can be achieved using existing control infrastructure is bounded by 4.5%. This prompts the potential of utilizing alternative actuators capable of controlling both high- and low-speed large-scale structures in the boundary layers. Furthermore, inspired by the results of Giovanetti *et al.* [7], there is also a possibility to target the LSMs and VLSMs closer to the wall with scales smaller than  $1.5\delta$  to further enhance the 8% DR limit, since it was shown that these scales contribute more to the generation of the mean wall-shear stress than the VLSMs or superstructures.

## Acknowledgement

Funding provided by the Australian Research Council is gratefully acknowledged.

## References

- [1] Abbassi, M.R., Baars, W.J., Hutchins, N., and Marusic, I., Skin-friction drag reduction in a high-Reynolds-number turbulent boundary layer via real-time control of large-scale structures, *Int. J. Heat Fluid Flow*, **67**, 2017, 30-41.
- [2] Baars, W.J., Talluru, K.M., Bishop, B.J., Hutchins, N., and Marusic, I., Spanwise inclination and meandering of large-scale structures in a high-Reynolds-number turbulent boundary layer, In 19th Australasian Fluid Mechanics Conference, 2014.
- [3] Baars, W.J., Hutchins, N., and Marusic, I., Spectral stochastic estimation of high-Reynolds-number wall-bounded turbulence for a refined inner-outer interaction model, *Phys. Rev. Fluids*, **1**(5), 2016, 054406.
- [4] Choi, H., Moin, P. and Kim, J. Active turbulence control for drag reduction in wall-bounded flows, *J. Fluid Mech.*, **262**, 1994, 75-110.
- [5] Deck, S., Renard, N., Laroche, R., and Weiss, P., Large-scale contribution to mean wall shear stress in high-Reynolds-number flat-plate boundary layers up to  $Re_\theta = 13650$ , *J. Fluid Mech.*, **743**, 2014, 202-248.
- [6] Gad-el-Hak, M., Interactive control of turbulent boundary layers-A futuristic overview, *AIAA J.*, **32**(9), 1994, 1753-1765.
- [7] de Giovanetti, M., Hwang, Y., and Choi, H., Skin-friction generation by attached eddies in turbulent channel flow, *J. Fluid Mech.*, **808**, 2016, 511-538.
- [8] Hutchins, N., and Marusic, I., Large-scale influences in near-wall turbulence, *Phil. Trans. R. Soc A*, **365**(1852), 2007 647-664.
- [9] Hutchins, N., Monty, J.P., Ganapathisubramani, B., Ng, H.C.H., and Marusic, I., Three-dimensional conditional structure of a high-Reynolds-number turbulent boundary layer, *J. Fluid Mech.*, **673**, 2011, 255-285.
- [10] Leschziner, M.A., Choi, H. and Choi, K.S. Flow-control approaches to drag reduction in aerodynamics: progress and prospects, *Phil. Trans. R. Soc A*, **369**, 2011, 1345-1351.
- [11] Mathis, R., Hutchins, N., and Marusic, I., Large-scale amplitude modulation of the small-scale structures in turbulent boundary layers, *J. Fluid Mech.*, **628**, 2009, 311-337.